Quantifying the Effect of Interfacial Dipoles on the Energy Level Alignment of Metal-Halide Perovskites

Luca Gregori,[a] Daniele Meggiolaro,[b] Filippo De Angelis[a,c,d] *

[a] *Department of Chemistry, Biology and Biotechnology, University of Perugia, Via Elce di Sotto 8, 06123, Perugia, Italy.*

[b] *Computational Laboratory for Hybrid/Organic Photovoltaics (CLHYO), Istituto CNR di Scienze e Tecnologie Chimiche "'Giulio Natta"' (CNR-SCITEC), Via Elce di Sotto 8, 06123 Perugia, Italy.*

[c] *Department of Natural Sciences & Mathematics, College of Sciences & Human Studies, Prince Mohammad Bin Fahd University, Dhahran, 34754 Saudi Arabia*

[d] *SKKU Institute of Energy Science and Technology (SIEST) Sungkyunkwan University, Suwon, 440-746 South Korea*

Corresponding Authors

Filippo De Angelis – filippo@thch.unipg.it

Abstract

Surface passivation with suitable organic molecules has emerged as an effective strategy to reduce surface defects and improve device efficiency. Adsorption of organic molecules on the MHPs surface, however, implies electrostatic and charge transfer interactions which may alter the energy levels of the underneath perovskite. Here, we elucidate the effects of differently functionalized anilines, as the prototype passivating molecule, on the electronic levels of the lead iodide perovskite at the surface by DFT calculations. While the nature of the surface-passivating molecules undoubtedly affects the dipole moment, we argue that the adsorption geometry and the extent of surface coverage plays an equally, if not more, important role in determining surface properties.

Graphics for Table of Contents

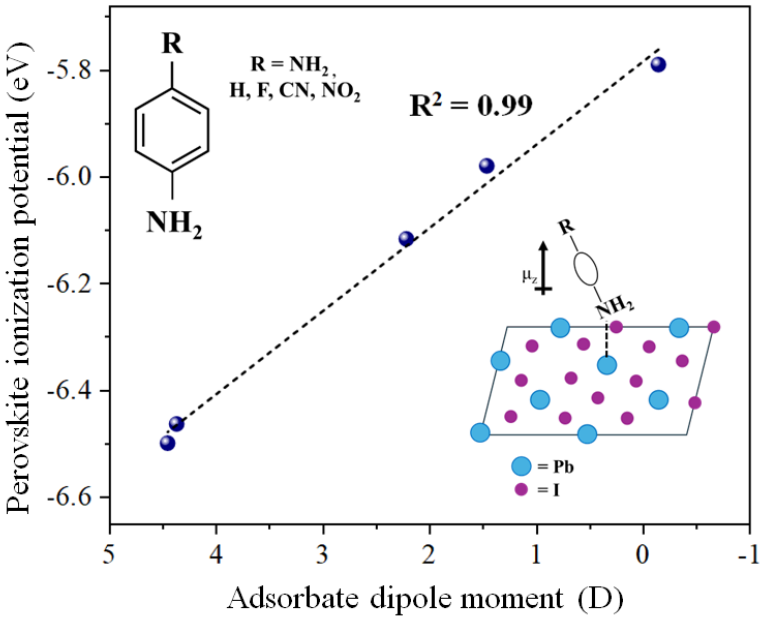

The remarkable properties of metal-halide perovskites (MHPs) make them promising candidates for various technological applications, including solar cells, light-emitting diodes, and catalysis.[1–4] The MHPs surface chemistry plays a crucial role in determining their performance and stability. [5] Surface passivation with suitable organic molecules has emerged as an effective strategy to reduce surface defects and improve device efficiency.[6] Adsorption of organic molecules on the MHPs surface, however, implies electrostatic and charge transfer interactions which may alter the energy levels of the underneath perovskite. In particular, the interplay between the adsorbate dipole moment and charge transfer is essential for the design of efficient passivation strategies. High dipole moments can induce polarization at the perovskite surface, leading to enhanced charge separation and reduced recombination rates. Conversely, the charge transfer between the passivating molecules and the perovskite surface must be carefully controlled to avoid unwanted doping effects or surface degradation.[7] Numerous studies have demonstrated the significance of interfacial dipoles in modulating the electronic properties and improving the performance of a range solar cells, ranging from perovskite to dye-sensitized to organic solar cells.[8–17] Engineering interfacial dipoles has been shown to enhance both the efficiency and stability of perovskite solar cells by improving band alignment, charge extraction, and reducing recombination losses.[18–32] In contrast to the conventional view, which often emphasizes the importance of the dipole moment on its own, our results reveal a more nuanced understanding.

In this study, based on density functional theory (DFT) calculations, we elucidate the effects of differently functionalized anilines, as the prototype passivating molecule, on the electronic levels of the lead iodide perovskite at the surface. As a first step, the energy of adsorption of the molecules on the PbI_2-terminated surface of MAPI has been studied. Hence, the trend between the molecular dipole, the associated charge transfer and the pinning of the perovskite levels is analyzed in order to rationalize the impact of these molecules on the charge extraction at the interlayer. Finally, the impact of molecular coverage for different terminations of the surface has been analyzed. While the nature of the surface-passivating molecule undoubtedly affects the dipole moment, we argue that

the adsorption geometry and the extent of surface coverage plays an equally, if not more, important role in determining surface properties.

To systematically investigate surface absorption properties and interfacial energy levels in MHPs, we consider the prototypical methylammonium lead iodide ($MAPbI_3$) perovskite. We calculate adsorption of various amount of passivating MAI groups and contrast these results to those obtained for functionalized anilines, see Figure 1, which allow us to systematically vary the adsorbate dipole moment by playing with aniline para substituents. From a technical side, we note that calculating molecular dipole moments can only be trustfully achieved for neutral systems, as the dipole moments of charged systems (*e.g.* methylammonium or formamidinium) are biased by the choice of the reference origin, giving rise to origin-dependent arbitrary numbers. As a matter of fact, reporting absolute values of dipole moments for charged species is essentially meaningless, thus we focus here on substituted anilines rather than on ammonium salts.

Aniline binds to lead ions at $MAPbI_3$ PbI_2-terminated surface (see schematics of adsorption in Figure 1b) through the $-NH_2$ group, while R substituents ($R=NH_2$, H, F, CN, NO_2) in para position have been selected in order to vary the dipole component perpendicularly to the surface (μ_z), which, incidentally, is the only dipole component relevant for shifting the energy levels. In Table 1 the dipole moments of the investigated molecules are reported, see computational details.

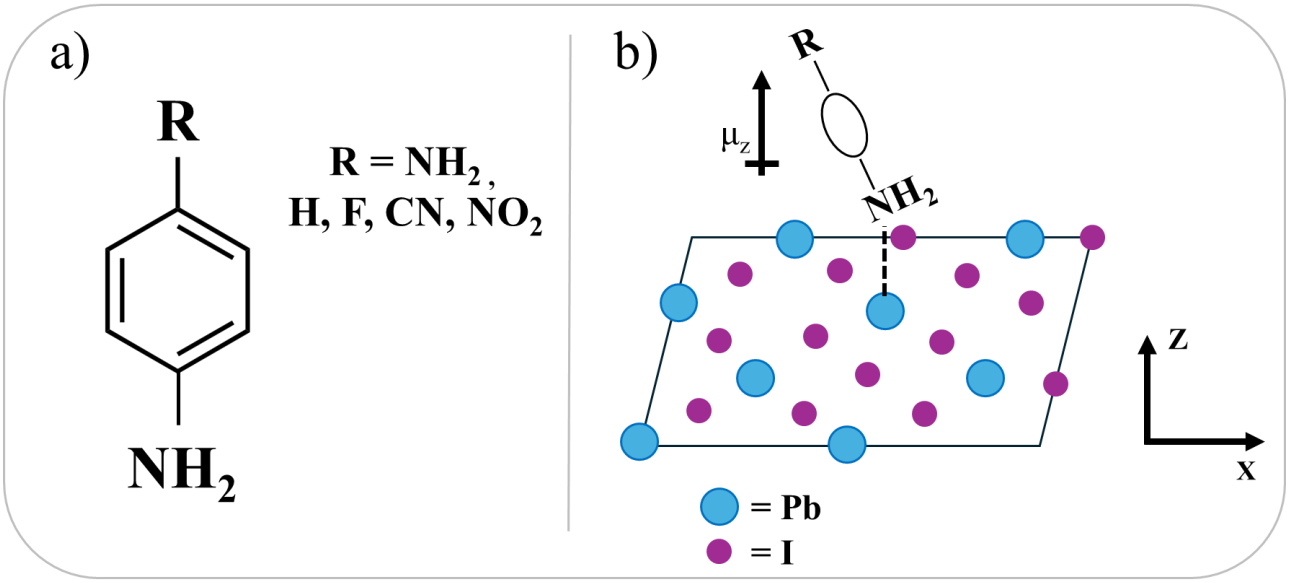

Figure 1. a) Chemical structure of the aniline derivatives analyzed in this work. b) Schematics of the $MAPbI_3$ (001) surface perovskite and definition of the reference for the dipole moment orientation used throughout the work.

As expected, the calculated dipole moments decrease by moving from $-NO_2$ to $-NH_2$ substituent, reflecting the decreasing electron withdrawing character of the different substituents. The explored range of the dipole moments varies from 4.45 Debye for R= $-NO_2$ (dipole pointing out from the surface in the +z direction) to -0.14 Debye in the case of $-NH_2$ (essentially zero dipole due to molecular symmetry). For clarity, here we use the dipole convention in which the vector points from the positive to the negative charge.

As a first step, the influence of the R substituent on the adsorption energies of the molecules on the PbI_2-terminated surface has been evaluated, see Table 1. Moving from $-NH_2$ to $-NO_2$ the adsorption energy progressively decreases, *i.e.* it becomes less negative, indicative of a weaker interaction between the molecule and the surface. This trend is a consequence of the redistribution of the electronic density on the aromatic ring induced by the different substituents. The $-NH_2$ group increases the electron density on the aromatic ring and as a consequence it stabilizes the bond

between the anchoring -NH_2 group and surface lead electronic states. On the other hand, electron-withdrawing groups (-F, -CN, -NO_2) decrease the electron density and destabilize the Pb-NH_2 interfacial bond.

Table 1. Calculated dipole moments perpendicular to the surface (μ_z) of the aniline derivatives; adsorption energies on the PbI_2-terminated surface; amount of transferred charge from the molecule to the perovskite upon adsorption; energy of the perovskite VBM with respect to the vacuum, set to zero.

Adsorbate aniline-R	**μ_z (Debye)**	**E_{ads} (eV)**	**Charge Transfer (electrons x 10^{-3})**	**VBM (eV)**
– NO_2	4.45	-0.71	0.33	-6.50
– CN	4.37	-0.74	0.37	-6.46
PbI_2-terminated surface	-	-	-	-6.34
- F	2.22	-0.86	0.39	-6.12
– H	1.46	-0.85	0.40	-5.98
- NH_2	-0.14	-0.96	0.43	-5.79

This is confirmed by the analysis of the electronic charge redistribution induced by the molecule upon adsorption on the surface. Single point DFT calculations have been performed on the slab and molecule fragments in the optimized adsorbed geometries and the difference in the electronic density between the fragments and the adsorbed system has been integrated in order to estimate the charge transfer into the perovskite slab upon adsorption. In Figure 2 the real space plots of the

charge redistribution upon adsorption are reported for the -NO_2 and -NH_2 substituents, as well as the associated planar average profiles along the z-direction. In Table 1 the integral of the transferred charge, *i.e.* the integral of the charge density difference between the blue dotted lines in Figure 2, are reported.

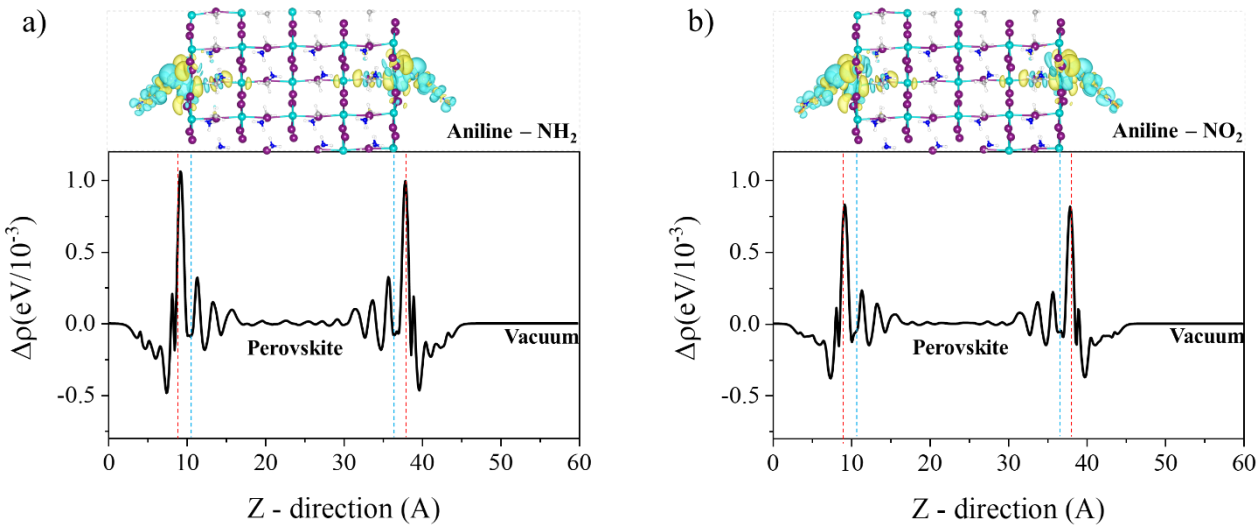

Figure 2. Real space plot of the charge redistribution upon adsorption and planar-average profile along the z-axis for the a) -NH_2 and b) -NO_2 substituents. In the real space plots the isosurface level has been set to 0.001 *e* per A^3, blue isosurface indicates a charge depletion, yellow isosurface indicates a charge accumulation. In the profile diagrams the perovskite slab boundaries are indicated by blue dotted lines, while the position of the -NH_2 nitrogen is indicated by the red dotted line.

As highlighted in Figure 2, electron charge density flows from the adsorbate aromatic ring to the perovskite outermost layer, due to the formation of the Pb-N bond at the interface. By looking at the integrated profile along the z-axis of the two substituents a limited charge transfer towards the perovskite surface is observed in the case of the -NO_2 substituent compared to -NH_2. Analysis of the transferred charge integrals in Table 1 and Figure S1 in supporting information shows a clear correlation between the electron-withdrawing character of the substituents and the charge transfer

into the perovskite, confirming that the adsorption of the aniline derivatives is more favorable for substituents increasing electron density in para position.

Hence, we move to discuss the impact of the molecule dipole moments on the electronic levels of the perovskite by monitoring the valence band maximum (VBM) energy of the perovskite slab in the different cases, see Table 1 and Figure 3. A linear decrease in the energy of the perovskite VBM with increasing the dipole moment of the molecule can be observed in Figure 3, with a linear correlation characterized by an R^2 value of 0.99. It should be noted that the adsorption of the examined molecules only slightly impacts the band gap of the perovskite, since deviations no larger than 0.09 eV with respect to the pristine surface were calculated, see Table S1 in SI. By focusing on the absolute values, a down-shift of the VBM energy is observed for the -NO_2 and -CN substituent compared to the bare PbI_2-terminated surface. On the contrary, an up-shift is reported for the -F, -H and -NH_2 substituents, highlighting that both charge transfer and dipole effects at the interface modulate the VBM energy of the perovskite substrate. Specifically, the -NH_2 substituent with close to zero dipole moment, induces an up-shift of the VBM of 0.55 eV compared to the bare surface. This is readily associated with the electron transfer induced by the molecule into the perovskite slab upon adsorption, as discussed above. By increasing the dipole moment of the molecule an opposite effect to the electron transfer is attained that linearly increases with the dipole magnitude, by leading to a VBM energy decrease of 0.15-0.16 eV for molecule with large dipole moments, *i.e.* -CN and -NO_2.

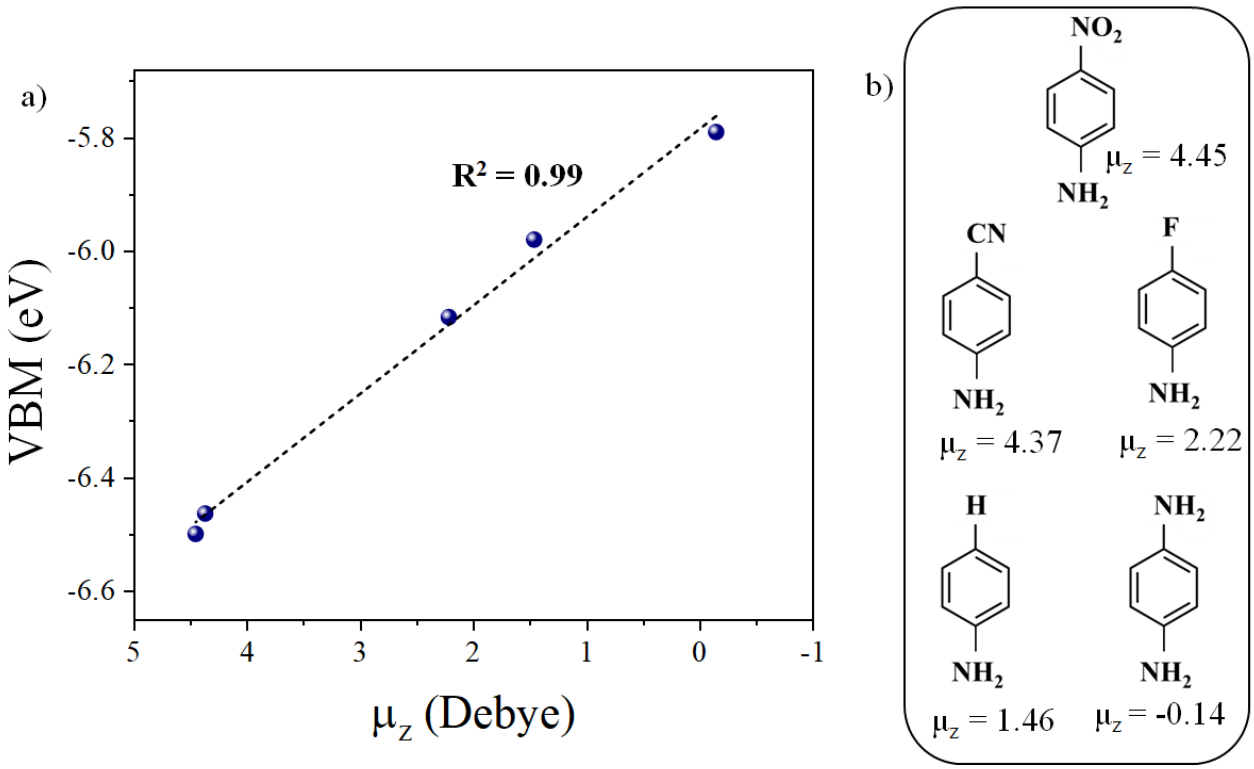

Figure 3. Valence band energy versus Dipole moment for the different aniline derivatives. b) Chemical structure and value of the calculated dipole moment for each of the derivatives.

So far, our DFT analysis highlights the combined role played by chemical passivation of under-coordinated lead ions and molecular dipoles in modulating the electronic levels of the perovskite at the surface. The linear decrease of the VBM by increasing the dipole moment of the molecule is in agreement with several experimental works reporting an increase of the work function induced by positive molecular dipoles at the perovskite surface.[27,28,31] Chemical passivation of lead ions at the surface, on the other hand, induces an increase of the VBM energy, indicating that the molecular surface coverage in parallel to surface dipoles strongly influence the final energy shift in the functionalized perovskite.

Hence, we move to analyze the effects of surface coverage on the different terminations of the surface. To this aim, we increased the passivation of the PbI_2-terminated surface by combining

aniline-derivatives with -NH_2, -H and -NO_2 substituents and MAI units up to the full coverage of the surface. Structural models of the analyzed systems are reported in Figure 4.

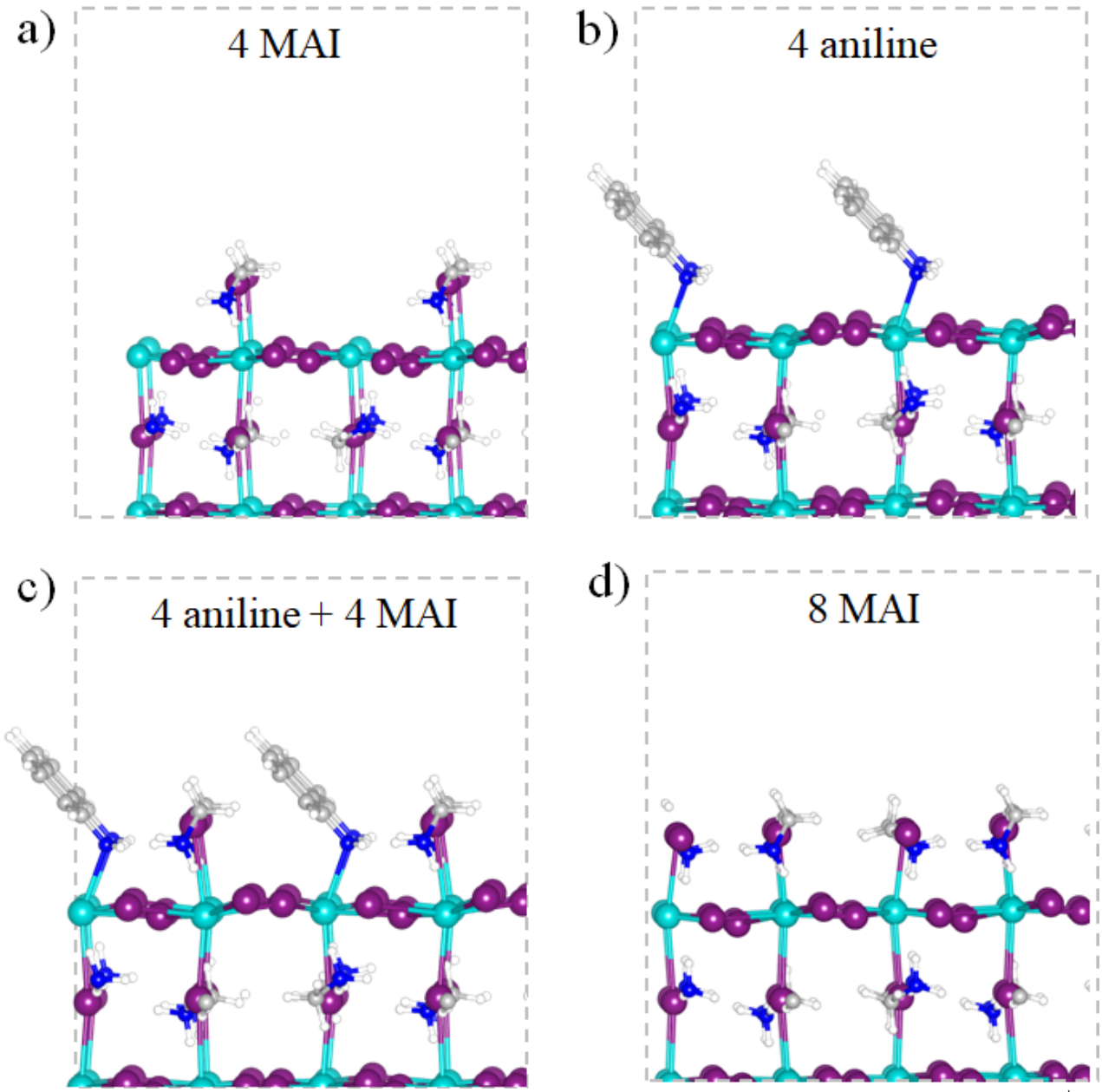

Figure 4. Optimized structure (reported for only one surface for clearness) for a) 4 units of MA^+-I^- salt ion pair. b) 4 units of aniline-R c) 4 units of MA^+-I^- salt ion pair and 4 units of Aniline-R e) full MA^+-I^- passivated surface. R= -NO_2, -H, -NH_2

In Table 2 the adsorption energies of the passivating units starting from the respective molecules and MAI units in vacuum are reported, to investigate the stability of the relative passivated surfaces. In agreement with previous works, [33] passivation leads to a stabilization of the PbI_2-terminated surface demonstrating a quasi-linear trend with the coverage (θ). By comparing the different passivating units, the adsorption of MAI is in all cases more favourable than that of the aniline substituents. The adsorption energy for one MAI unit was found to be -1.81 eV, indicating strong interaction and effective passivation. In comparison, the adsorption energy for one aniline-NH_2 molecule, which shows the highest adsorption energy among the considered substituents, was -0.90 eV which, while still thermodynamically possible, suggests a weaker interaction with the substrate

Table 2. Interaction energy for the substituted aniline adsorbed systems and ionization energy.

System	**E_{ads} (eV)**	**Valence Band Energy (eV)**
PbI_2-terminated surface (θ = 0.0)	/	-6.34
4 MAI (θ = 0.5)	-1.85	-5.44
8 MAI (θ = 1.0)	-2.11	-4.94
4 aniline-NO_2	-0.75	-6.88
4 aniline-H	-0.83	-5.46
4 aniline-NH_2	-0.90	-4.72
4 MAI + 4 aniline-NO_2	-1.36	-6.24
4 MAI + 4 aniline-H	-1.43	-4.94
4MAI + 4 aniline-NH_2	-1.47	-4.65

By looking at the VBM energies, starting from the PbI_2-terminated surface the passivation with MAI and aniline-H leads to a very similar up-shift of the VBM vs the coverage, see Table 2 and

Figure 5. The -NH_2 substituent, carrying a nearly zero dipole moment, while following the same trend with the coverage, leads to a further increase of the VBM, in agreement with the charge transfer analysis. Notably, the VBM energy up-shift observed for four passivating units is only slightly higher than for a single unit, indicating a relatively quick degree of saturation. The -NO_2 substituent has the opposite effect, by leading to a stabilization of the VBM and to a modest saturation rate with the coverage. In this analysis the combined effects of chemical passivation and the dipoles at the surface clearly emerge. Starting from the PbI_2-terminated surface, the chemical saturation of surface leads and the electron transfer upon adsorption drive the up-shift of the perovskite VBM, while molecular dipoles pointing outwards from the surface lead to a parallel down-shift of the VBM.

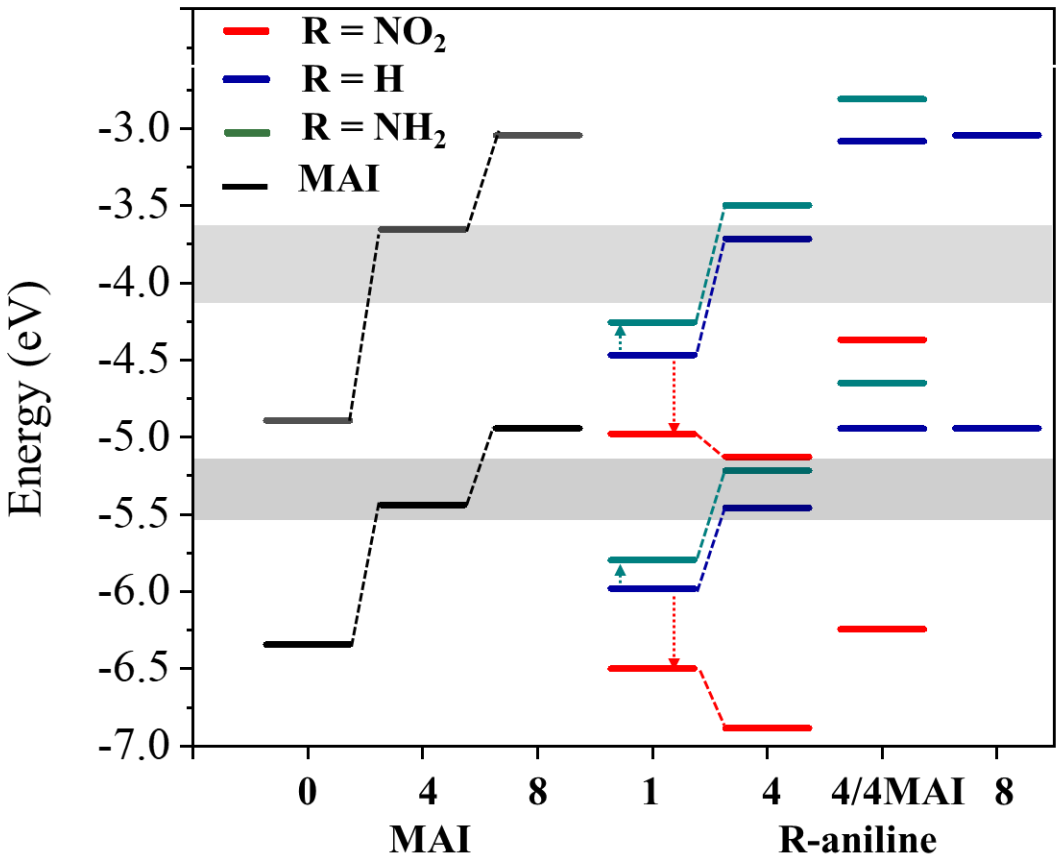

Figure 5. Calculated energy levels as a function of MAI passivation and of substituted aniline (R-aniline) coverage. The energy range of typical ETLs and HTLs are also indicated as shaded grey areas.

It is interesting to compare the calculated VBM in the different cases with the position of most common HTL and ETL used in devices, see Figure 5. The higher stability of the MAI passivated surface suggests that MAI coverage between 0.5 and 1.0 are expected in standard polycrystalline samples. This is indeed in line with typical measured VBM values for $MAPbI_3$ of ~-5.5 eV. [33] Based on our simulations, for MAI-rich surfaces the VBM is resonant or slightly higher in energy than typical energy levels of HTLs, suggesting that post-treatment with polar molecules with electron-withdrawing functional groups may improve the alignment at the interface, in turn affecting the efficiency of charge extraction in solar cells.

In summary, we have quantified the effect of electrostatic and charge transfer interactions in determining interfacial energy levels in metal-halide perovskites. By systematically investigating a series of para-substituted anilines we have been able to trustfully determine the relation between adsorbate electronic properties and alignment of energy levels at the perovskite interface. Our results reveal the interplay of adsorption geometry, binding energy and electronic properties of the adsorbates in determining such energy shifts. Importantly, the competition between iodide precursors salts, *i.e.* MAI or FAI, and substituted anilines in binding to the perovskite surface has been highlighted, which is fundamental in determining the actual energy shifts due to the subtle dependence on coverage. We hope our results will be useful in rationalizing the widespread use of molecular adsorbate to tune the perovskite energy levels.

Acknowledgements

Funded by the European Union. Views and opinions expressed are however those of the author(s) only and do not necessarily reflect those of the European Union or CINEA. Neither the European Union nor the granting authority can be held responsible for them. VALHALLA project has received funding from Horizon Europe Research and Innovation Action programme under Grant Agreement nº 101082176.

This work has been also funded by the European Union - NextGenerationEU under the Italian Ministry of University and Research (MUR) National Innovation Ecosystem grant ECS00000041 -

VITALITY - CUP J97G22000170005 and CUP: B43C22000470005. The authors acknowledge Università degli Studi di Perugia and MUR for support within the project Vitality.

References

(1) Kojima, A.; Teshima, K.; Shirai, Y.; Miyasaka, T. Organometal Halide Perovskites as Visible-Light Sensitizers for Photovoltaic Cells. *J. Am. Chem. Soc.* **2009**, *131* (17), 6050–6051. https://doi.org/10.1021/ja809598r.
(2) Lee, M. M.; Teuscher, J.; Miyasaka, T.; Murakami, T. N.; Snaith, H. J. Efficient Hybrid Solar Cells Based on Meso-Superstructured Organometal Halide Perovskites. *Science* **2012**, *338* (6107), 643–647. https://doi.org/10.1126/science.1228604.
(3) Kim, H.-S.; Lee, C.-R.; Im, J.-H.; Lee, K.-B.; Moehl, T.; Marchioro, A.; Moon, S.-J.; Humphry-Baker, R.; Yum, J.-H.; Moser, J. E.; Grätzel, M.; Park, N.-G. Lead Iodide Perovskite Sensitized All-Solid-State Submicron Thin Film Mesoscopic Solar Cell with Efficiency Exceeding 9%. *Sci. Rep.* **2012**, *2* (1), 591. https://doi.org/10.1038/srep00591.
(4) Chung, I.; Lee, B.; He, J.; Chang, R. P. H.; Kanatzidis, M. G. All-Solid-State Dye-Sensitized Solar Cells with High Efficiency. *Nature* **2012**, *485* (7399), 486–489. https://doi.org/10.1038/nature11067.
(5) Yang, S.; Chen, S.; Mosconi, E.; Fang, Y.; Xiao, X.; Wang, C.; Zhou, Y.; Yu, Z.; Zhao, J.; Gao, Y.; De Angelis, F.; Huang, J. Stabilizing Halide Perovskite Surfaces for Solar Cell Operation with Wide-Bandgap Lead Oxysalts. *Science* **2019**, *365* (6452), 473–478. https://doi.org/10.1126/science.aax3294.
(6) Suo, J.; Yang, B.; Mosconi, E.; Bogachuk, D.; Doherty, T. A. S.; Frohna, K.; Kubicki, D. J.; Fu, F.; Kim, Y.; Er-Raji, O.; Zhang, T.; Baldinelli, L.; Wagner, L.; Tiwari, A. N.; Gao, F.; Hinsch, A.; Stranks, S. D.; De Angelis, F.; Hagfeldt, A. Multifunctional Sulfonium-Based Treatment for Perovskite Solar Cells with Less than 1% Efficiency Loss over 4,500-h Operational Stability Tests. *Nat. Energy* **2024**, *9* (2), 172–183. https://doi.org/10.1038/s41560-023-01421-6.
(7) Ronca, E.; Pastore, M.; Belpassi, L.; Tarantelli, F.; Angelis, F. D. Influence of the Dye Molecular Structure on the TiO2 Conduction Band in Dye-Sensitized Solar Cells: Disentangling Charge Transfer and Electrostatic Effects. *Energy Environ. Sci.* **2012**, *6* (1), 183–193. https://doi.org/10.1039/C2EE23170K.
(8) De Angelis, F.; Fantacci, S.; Selloni, A.; Grätzel, M.; Nazeeruddin, M. K. Influence of the Sensitizer Adsorption Mode on the Open-Circuit Potential of Dye-Sensitized Solar Cells. *Nano Lett.* **2007**, *7* (10), 3189–3195. https://doi.org/10.1021/nl071835b.
(9) Chen, Q.; Wang, C.; Li, Y.; Chen, L. Interfacial Dipole in Organic and Perovskite Solar Cells. *J. Am. Chem. Soc.* **2020**, *142* (43), 18281–18292. https://doi.org/10.1021/jacs.0c07439.
(10) *Enhanced power-conversion efficiency in polymer solar cells using an inverted device structure | Nature Photonics*. https://www.nature.com/articles/nphoton.2012.190 (accessed 2024-05-30).
(11) *A Universal Method to Produce Low–Work Function Electrodes for Organic Electronics | Science*. https://www.science.org/doi/10.1126/science.1218829 (accessed 2024-05-30).
(12) *A Semi-transparent Plastic Solar Cell Fabricated by a Lamination Process - Huang - 2008 - Advanced Materials - Wiley Online Library*. https://onlinelibrary.wiley.com/doi/10.1002/adma.200701101 (accessed 2024-05-30).
(13) Zuo, L.; Gu, Z.; Ye, T.; Fu, W.; Wu, G.; Li, H.; Chen, H. Enhanced Photovoltaic Performance of CH3NH3PbI3 Perovskite Solar Cells through Interfacial Engineering Using Self-Assembling Monolayer. *J. Am. Chem. Soc.* **2015**, *137* (7), 2674–2679. https://doi.org/10.1021/ja512518r.
(14) Azmi, R.; Hadmojo, W. T.; Sinaga, S.; Lee, C.-L.; Yoon, S. C.; Jung, I. H.; Jang, S.-Y. High-Efficiency Low-Temperature ZnO Based Perovskite Solar Cells Based on Highly Polar,

Nonwetting Self-Assembled Molecular Layers. *Adv. Energy Mater.* **2018**, *8* (5), 1701683. https://doi.org/10.1002/aenm.201701683.
(15) Choi, H.; Kim, H.-B.; Ko, S.-J.; Kim, J. Y.; Heeger, A. J. An Organic Surface Modifier to Produce a High Work Function Transparent Electrode for High Performance Polymer Solar Cells. *Adv. Mater.* **2015**, *27* (5), 892–896. https://doi.org/10.1002/adma.201404172.
(16) Cheng, Y.; Li, M.; Liu, X.; Cheung, S. H.; Chandran, H. T.; Li, H.-W.; Xu, X.; Xie, Y.-M.; So, S. K.; Yip, H.-L.; Tsang, S.-W. Impact of Surface Dipole in NiOx on the Crystallization and Photovoltaic Performance of Organometal Halide Perovskite Solar Cells. *Nano Energy* **2019**, *61*, 496–504. https://doi.org/10.1016/j.nanoen.2019.05.004.
(17) Zhang, M.; Chen, Q.; Xue, R.; Zhan, Y.; Wang, C.; Lai, J.; Yang, J.; Lin, H.; Yao, J.; Li, Y.; Chen, L.; Li, Y. Reconfiguration of Interfacial Energy Band Structure for High-Performance Inverted Structure Perovskite Solar Cells. *Nat. Commun.* **2019**, *10* (1), 4593. https://doi.org/10.1038/s41467-019-12613-8.
(18) Qiu, Y.; Liang, J.; Zhang, Z.; Deng, Z.; Xu, H.; He, M.; Wang, J.; Yang, Y.; Kong, L.; Chen, C.-C. Tuning the Interfacial Dipole Moment of Spacer Cations for Charge Extraction in Efficient and Ultrastable Perovskite Solar Cells. *J. Phys. Chem. C* **2021**, *125* (2), 1256–1268. https://doi.org/10.1021/acs.jpcc.0c09606.
(19) Liu, Y.; Akin, S.; Pan, L.; Uchida, R.; Arora, N.; Milić, J. V.; Hinderhofer, A.; Schreiber, F.; Uhl, A. R.; Zakeeruddin, S. M.; Hagfeldt, A.; Dar, M. I.; Grätzel, M. Ultrahydrophobic 3D/2D Fluoroarene Bilayer-Based Water-Resistant Perovskite Solar Cells with Efficiencies Exceeding 22%. *Sci. Adv.* **2019**, *5* (6), eaaw2543. https://doi.org/10.1126/sciadv.aaw2543.
(20) Dong, H.; Xi, J.; Zuo, L.; Li, J.; Yang, Y.; Wang, D.; Yu, Y.; Ma, L.; Ran, C.; Gao, W.; Jiao, B.; Xu, J.; Lei, T.; Wei, F.; Yuan, F.; Zhang, L.; Shi, Y.; Hou, X.; Wu, Z. Conjugated Molecules "Bridge": Functional Ligand toward Highly Efficient and Long-Term Stable Perovskite Solar Cell. *Adv. Funct. Mater.* **2019**, *29* (17), 1808119. https://doi.org/10.1002/adfm.201808119.
(21) Tan, S.; Zhou, N.; Chen, Y.; Li, L.; Liu, G.; Liu, P.; Zhu, C.; Lu, J.; Sun, W.; Chen, Q.; Zhou, H. Effect of High Dipole Moment Cation on Layered 2D Organic–Inorganic Halide Perovskite Solar Cells. *Adv. Energy Mater.* **2019**, *9* (5), 1803024. https://doi.org/10.1002/aenm.201803024.
(22) Liu, H.; Lu, Z.; Zhang, W.; Wang, J.; Lu, Z.; Dai, Q.; Qi, X.; Shi, Y.; Hua, Y.; Chen, R.; Shi, T.; Xia, H.; Wang, H.-L. Anchoring Vertical Dipole to Enable Efficient Charge Extraction for High-Performance Perovskite Solar Cells. *Adv. Sci.* **2022**, *9* (29), 2203640. https://doi.org/10.1002/advs.202203640.
(23) Chen, W.; Liu, S.; Li, Q.; Cheng, Q.; He, B.; Hu, Z.; Shen, Y.; Chen, H.; Xu, G.; Ou, X.; Yang, H.; Xi, J.; Li, Y.; Li, Y. High-Polarizability Organic Ferroelectric Materials Doping for Enhancing the Built-In Electric Field of Perovskite Solar Cells Realizing Efficiency over 24%. *Adv. Mater.* **2022**, *34* (14), 2110482. https://doi.org/10.1002/adma.202110482.
(24) Wang, J.; Li, J.; Zhou, Y.; Yu, C.; Hua, Y.; Yu, Y.; Li, R.; Lin, X.; Chen, R.; Wu, H.; Xia, H.; Wang, H.-L. Tuning an Electrode Work Function Using Organometallic Complexes in Inverted Perovskite Solar Cells. *J. Am. Chem. Soc.* **2021**, *143* (20), 7759–7768. https://doi.org/10.1021/jacs.1c02118.
(25) Zhang, C.; Kong, W.; Wu, T.; Lin, X.; Wu, Y.; Nakazaki, J.; Segawa, H.; Yang, X.; Zhang, Y.; Wang, Y.; Han, L. Reduction of Nonradiative Loss in Inverted Perovskite Solar Cells by Donor−π–Acceptor Dipoles. *ACS Appl. Mater. Interfaces* **2021**, *13* (37), 44321–44328. https://doi.org/10.1021/acsami.1c11683.
(26) Zhang, J.; Hu, H.; Zhang, Y.; Liang, Z.; Zhu, P.; Li, Z.; Wang, D.; Chen, J.; Zeng, J.; Jiang, Z.; Wu, J.; Zhang, L.; Hu, B.; Pan, X.; Wang, X.; Xu, B. Tuning Perovskite Surface Polarity via Dipole Moment Engineering for Efficient Hole-Transport-Layer-Free Sn–Pb Mixed-Perovskite Solar Cells. *ACS Appl. Mater. Interfaces* **2023**, *15* (12), 15321–15331. https://doi.org/10.1021/acsami.2c20915.

(27) Li, T.; Xu, J.; Lin, R.; Teale, S.; Li, H.; Liu, Z.; Duan, C.; Zhao, Q.; Xiao, K.; Wu, P.; Chen, B.; Jiang, S.; Xiong, S.; Luo, H.; Wan, S.; Li, L.; Bao, Q.; Tian, Y.; Gao, X.; Xie, J.; Sargent, E. H.; Tan, H. Inorganic Wide-Bandgap Perovskite Subcells with Dipole Bridge for All-Perovskite Tandems. *Nat. Energy* **2023**, *8* (6), 610–620. https://doi.org/10.1038/s41560-023-01250-7.
(28) Teng, T.-Y.; Su, Z.-H.; Hu, F.; Chen, C.-H.; Chen, J.; Wang, K.-L.; Xue, D.; Gao, X.-Y.; Wang, Z.-K. Electronically Manipulated Molecular Strategy Enabling Highly Efficient Tin Perovskite Photovoltaics. *Angew. Chem.* **2024**, *136* (7), e202318133. https://doi.org/10.1002/ange.202318133.
(29) Zhou, Q.; Zuo, C.; Zhang, Z.; Gao, P.; Ding, L. F-Containing Cations Improve the Performance of Perovskite Solar Cells. *J. Semicond.* **2022**, *43* (1), 010202. https://doi.org/10.1088/1674-4926/43/1/010202.
(30) Shi, Y.; Zhu, Z.; Miao, D.; Ding, Y.; Mi, Q. Interfacial Dipoles Boost Open-Circuit Voltage of Tin Halide Perovskite Solar Cells. *ACS Energy Lett.* **2024**, *9* (4), 1895–1897. https://doi.org/10.1021/acsenergylett.4c00529.
(31) Canil, L.; Cramer, T.; Fraboni, B.; Ricciarelli, D.; Meggiolaro, D.; Singh, A.; Liu, M.; Rusu, M.; Wolff, C. M.; Phung, N.; Wang, Q.; Neher, D.; Unold, T.; Vivo, P.; Gagliardi, A.; De Angelis, F.; Abate, A. Tuning Halide Perovskite Energy Levels. *Energy Environ. Sci.* **2021**, *14* (3), 1429–1438. https://doi.org/10.1039/D0EE02216K.
(32) Duan, J.; Wang, M.; Wang, Y.; Zhang, J.; Guo, Q.; Zhang, Q.; Duan, Y.; Tang, Q. Effect of Side-Group-Regulated Dipolar Passivating Molecules on $CsPbBr_3$ Perovskite Solar Cells. *ACS Energy Lett.* **2021**, *6* (6), 2336–2342. https://doi.org/10.1021/acsenergylett.1c01060.
(33) Meggiolaro, D.; Mosconi, E.; Proppe, A. H.; Quintero-Bermudez, R.; Kelley, S. O.; Sargent, E. H.; De Angelis, F. Energy Level Tuning at the $MAPbI_3$ Perovskite/Contact Interface Using Chemical Treatment. *ACS Energy Lett.* **2019**, *4* (9), 2181–2184. https://doi.org/10.1021/acsenergylett.9b01584.